



# Violin String Inspired Core-Sheath Silk/Steel Yarns for Wearable Triboelectric Nanogenerator Applications

Chao Ye<sup>1</sup> · Quanfu Xu<sup>2</sup> · Jing Ren<sup>1</sup> · Shengjie Ling<sup>1</sup>

Received: 11 November 2019 / Revised: 13 December 2019 / Accepted: 14 December 2019 / Published online: 22 January 2020  
© Donghua University, Shanghai, China 2020

## Abstract

Triboelectric nanogenerator (TENG) has attracted considerable attention in wearable electronics and energy harvesting associated with human activities. Fiber/yarn electrodes are widely applied in the wearable TENG system, which remains a challenge to guarantee mechanical ductility and stable electrical functions during long-term use. Inspired by high quality violin strings core-sheath design, silk/stainless-steel integrated yarns (SSYs) are continuously produced by simple co-wrapping spinning technique, which shows excellent mechanical strength, flexibility, conductivity, weaveability and triboelectric function. The SSYs can be modified to achieve tunable surface morphology. Finally, TENG cables have been fabricated, which can be stretched up to 100% and reveal a fast responsiveness to the stretching extent (voltage output of about 0.2, 0.6, 1.8, 2.8 V at 13%, 25%, 38%, 50% stretching, respectively). The TENG cables integrated textiles can not only harvest the energy generated by body movement but can also work as a self-supplied motion detector.

**Keywords** Silk · Fiber · Triboelectric nanogenerator · Wearable energy devices

## Introduction

Wearable devices integrated smart-textiles and multifunctional suits are receiving significant research enthusiasm due to the urgent needs of constantly monitoring human body condition to prevent disease and provide extra protection, and other promising future applications such as body function enhancement [1–3]. Power supply for these integrated intelligent clothing remains a challenge. A lot of researches have been demonstrated in flexible energy storage devices to replace traditional rigid battery packs as power sources, such

as a various of fiber-shaped and thin-film electrochemical energy storage devices [4–7]. These designed energy storage devices can provide record-breaking high energy density; however, their total capacity was compromised due to the low material loading. One essential point of wearable devices is to achieve light weight, comfortability and convenience when worn on the curved human body. Therefore, the energy supply still remains a bottleneck hindering the progress of wearable electronics.

The idea of real-time energy harvesting provides a promising solution. Wearable energy-harvesting and energy-storing devices can be integrated into a self-sustainable power system [8]. For example, wearable solar cells are developed to harvest solar energy at daytime [9, 10]. However, they are vulnerable to the environment, and are invalid when being sheltered during body movement. On the other hand, triboelectric nanogenerator (TENG) has attracted considerable attention in wearable electronics and the internet-of-things for harvesting mechanical energy associated with human activities [11–13]. Compared with conventional electromagnetic generators, TENGs feature advantages in lightweight, wide choice of materials and effectiveness in low-frequency energy harvesting [14].

Wearable TENGs usually appear as textiles, constructed by integrating polymer fibers/fabrics (such as nylon/

**Electronic supplementary material** The online version of this article (<https://doi.org/10.1007/s42765-019-00023-w>) contains supplementary material, which is available to authorized users.

✉ Jing Ren  
renjing@shanghaitech.edu.cn

✉ Shengjie Ling  
lingshj@shanghaitech.edu.cn

<sup>1</sup> School of Physical Science and Technology, ShanghaiTech University, 393 Middle Huaxia Road, Shanghai 201210, China

<sup>2</sup> Department of Cardiology, Xinhua Hospital, School of Medicine, Shanghai Jiao Tong University, 200092 Shanghai, China

polyester fabric and cotton fiber) [15–17] with conductive nanomaterials (such as carbon nanotube, gold nanoparticles and silver nanowire) [15, 16, 18]. Thus, fiber/yarn electrodes which can be used directly or weaving into textiles are widely applied in the wearable TENG system. In most of these fiber/yarn electrodes, combinations between the polymer and conductive materials are often achieved through solution coating, deposition or co-textile technique. It is still a challenge to guarantee mechanical ductility and stable electrical functions during long-term repeated bending, curving and rubbing. In this regard, Violin strings can provide inspiration. For example, high-quality violin strings often achieve a superior toughness, high structure stability and preferred friction with bow, by wrapping nylon fiber around carbon steel wire core [19]. This design strategy can be introduced to produce improved integrated polymer/metal yarn electrode for wearable electronic device applications.

Herein, violin strings inspired silk/stainless-steel integrated yarns (SSYs) were continuously produced by simple co-wrapping spinning technique. The stainless-steel core fiber provides excellent mechanical strength, flexibility and conductivity, while the helical silk fiber sheath provides triboelectric function. The surface of SSYs can be modified to form a glued interface between silk fibers by solvent treatment, or to introduce nanostructures through reactive ion etching (RIE). The former enhances the SSY's structure stability, while the latter increases its specific surface area. Therefore, the prepared SSYs were assembled into stretchable TENG cables, which can be used as an energy harvester to collect mechanical energy. The flexible TENG cables can be stretched up to 100%, also reveal a fast responsiveness to the stretching extent (voltage output of about 0.2, 0.6, 1.8, 2.8 V at 13%, 25%, 38%, 50% stretching, respectively). Further, the TENG cables integrated textiles can not only harvest the energy generated by body movement at any time but can also work as a self-supplied sensor for motion monitoring.

## Experimental Section

### Preparation of SSYs

Commercial silk yarn (~150  $\mu\text{m}$  in diameter) and stainless-steel yarn (~200  $\mu\text{m}$  in diameter) (Fig. S1) were selected as raw materials to fabricate SSYs. A custom made co-wrapping spinning apparatus was used for fabricating SSYs. The apparatus is composed of three key parts. The first part is a feeding motor to provide the core fibers, the second is a co-wrapping system made by a rotator and a force controller, the third part is a motor-based collecting system. During the co-wrapping spinning, the wrap angle, namely, wrapping density of sheath yarns, can be modulated by changing

the speed ratio between the drawing speed of core fiber. In typical processing of SSYs, the speed of wrapping unit and speed of drawing unit were fixed at 700 rpm and 120  $\text{mm min}^{-1}$  to obtain full-packaged core-sheath yarns, respectively. The resultant SSYs show a structure of yarn spun with ~5800 turns  $\text{m}^{-1}$  and no gaps between the sheath silk fibers.

### Modification of SSYs by Hexafluoroisopropanol (HFIP) Incubation

Firstly, length of ~10 m of the obtained SSYs were placed into 20 mL glass bottles. Then, 15 mL HFIP was added into the glass bottles and the SSYs were immersed in HFIP solution. The modified SSYs were obtained after incubating in airtight containers as mixtures at 60 °C for 7 days, 14 days and 28 days, respectively. The residual solvent was removed thoroughly by drying the fibers at room temperature for 1 day. All of these steps were conducted in a chemical hood with the necessary precautions since HFIP is a toxic solvent.

### Fabrication of Nanowires Array on SSYs Surface

The reactive ion etching (RIE) (Plasma-Therm, Advanced Vacuum, Sweden) was used to fabricate the aligned nanowires on the SSYs surface.  $\text{O}_2$  gases was injected into the RIE chamber with flow ratio of 60.0 sccm. A large density of plasma was produced by a power source of 100 W. The surface of obtained SSYs feature with nanowires array structure after 5–30 min continuous etching. The length of the nanowires increases with the increasing of processing time.

## Characterization of SSYs

### Structure and Morphologies

SSYs and modified SSYs were observed by high-resolution scanning electron microscope (SEM, JEOL JSM-7800F, Tokyo, Japan) at an acceleration voltage of 5 kV. Samples were coated with a 5 nm thick gold layer to provide conductivity before observation.

### Tensile Measurements

Mechanical properties of SSYs and modified SSYs were tested by Instron 5966 machine (Instron, Norwood, USA). The SSYs were first cut into 40 mm segments for tensile tests. The 40 mm segments were mounted onto the Instron 5966 machine. Meanwhile, the initial length of the fiber was measured with a caliper at zero load point (the point in which the yarns are tight, but no force exerted on it). All

the tensile tests were carried out at 22 °C and 50% relative humidity with a tensile speed of 0.5 mm min<sup>-1</sup>.

### Fabrication of the Stretchable TENG Cables

Commercial silicone rubber tubes with inner diameter of 3 mm and outer diameter of 4 mm were used for the fabrication of the sheath fiber tube of the TENG cables. Firstly, the silicone rubber tubes were pre-stretched to twice its original length, followed by wrapping a copper fiber on the surface of the pre-stretched silicone rubber tube. Meanwhile, a core SSY was inserted into the sheath rubber tube. Then, the stretchable TENG cables were obtained by releasing the pre-stretched silicone rubber tubes together with the inserted SSY back to its original state.

### Characterization of the Stretchable TENG Cables

#### Electric Measurements

A home-made liner motor was applied to stretch the tested TENG cable with controlled speed and stretch extent. An electrochemical workstation (CHI660E, Shanghai Chenhua Instruments, China) was used to measure the output voltages at an external load of 500 MΩ and short-circuit currents of the stretchable TENG cables. The output

performance of the TENG cables was tested at relative humidity of 50%.

## Results

### Violin Strings Inspired SSYs

Nylon and steel wires wrapped with metal are commonly applied for violin strings of G, D and A (Fig. 1a, b), which provide smooth, thick or light tones and good durability. As the most important instrument in the string group of a modern orchestra, violin makes a sound by rubbing the string against the bow. Ancient violin strings were originally bare strings made of sheep's intestines, suffered from poor durability and the sound was always influenced by the environment. From 18th century, the bass G string was wrapped with silver wire, making it more responsive. Violin makers have realized that the mechanical properties, surface microstructure and stability of strings would all influence the quality and sound of the instrument. The inner core wire provides good mechanical strength and toughness, while the outer sheath wire provides appropriate friction with bow. The integrated strings perform preferred vibration frequency and are much more stable than the ancient strings during long-term performing.

Inspired by the modern violin strings design, SSYs are continuously produced by wrapping silk fibers onto a stainless-steel fiber core through co-wrapping spinning

**Fig. 1** Preparation method of violin strings inspired SSYs. **a** Image of a typical violin. Inset is cross-section SEM image of a violin A string (Pirastro TONICA, Germany), red circle indicating the core fiber. **b** SEM image of a typical integrated nylon/aluminum metal wire for A strings (Pirastro TONICA, Germany). **c** Schematic of co-wrapping spinning technique. **d** A roll of SSYs produced by the device shown in (c). **e** SEM image demonstrating surface morphology of a typical SSY

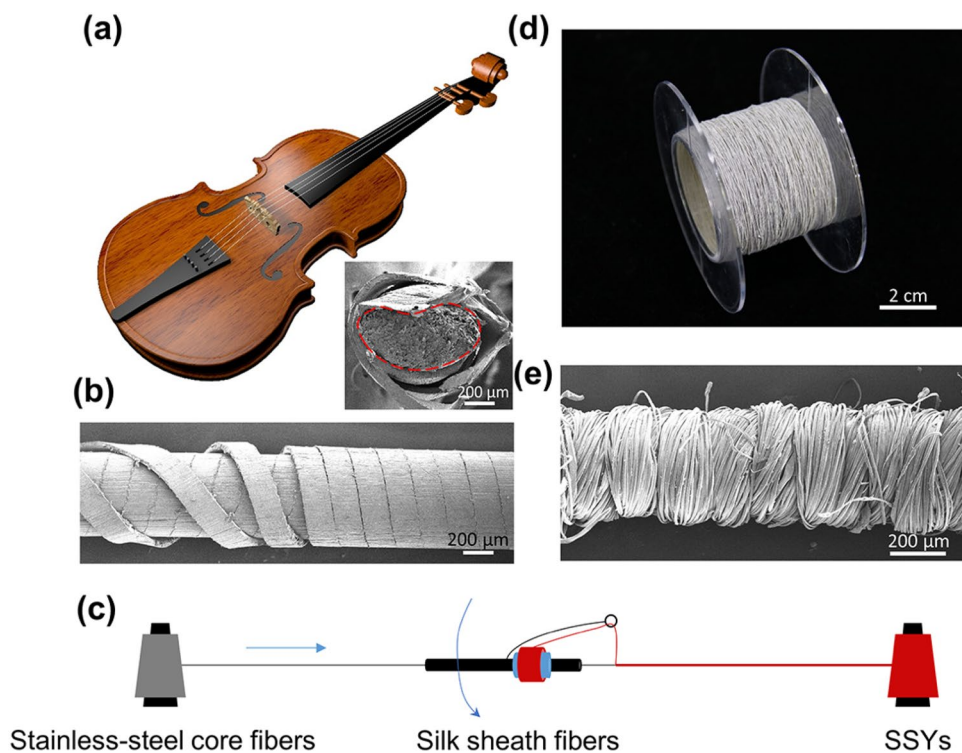


(Fig. 1c), which is a mature technology in the textile industry. Therefore, a roll of SSYs with a length of 22 m can be collected within 3 h (Fig. 1d). During the spinning process, the stainless-steel fibers pass through the hollow tube at a certain speed, which is controlled by the drawing rollers. A metal rotor loaded with silk fibers rotated counterclockwise. Changing the drawing speed ratios between the drawing speed of the core fiber and the rotating speed of the wrapper fibers can tailor the angle and wrap intensity. The inner stainless-steel fiber core is not expected to be exposed when the SSYs are under intense deformation and pulling. In this work, the most intensive strategy was applied to achieve a compact winding, where drawing speed/rotating speed was fixed at  $120 \text{ mm min}^{-1}$  and 700 rpm, respectively. The resulted wrapping angle is almost  $90^\circ$  (Fig. 1e).

## The Surface Modification of SSYs

The surface morphology of the SSYs were optimized through partial dissolution and RIE treatment of the helical silk fiber layers. The partial dissolution process can be achieved by incubating the SSYs in hexafluoroisopropanol (HFIP) solution [20–22]. With this process, the silk fibers in the sheath layer were dissolved into microfibrils by HFIP. The dissolved silk proteins then acted as a solid glue to fill the gaps between silk fibers and join the silk fibers together (Fig. 2a, b). Since HFIP is a mild solvent to dissolve silk fibers, the dissolution extent of silk layer can be easily controlled by the incubating time. Figure S2 shows the morphology of the surface of SSYs after incubated in HFIP solvent at  $60^\circ \text{C}$  for 7, 14 and 28 days, respectively.

With the increased incubating time in HFIP, helical microstructures formed by the wrapped silk fibers at the SSY

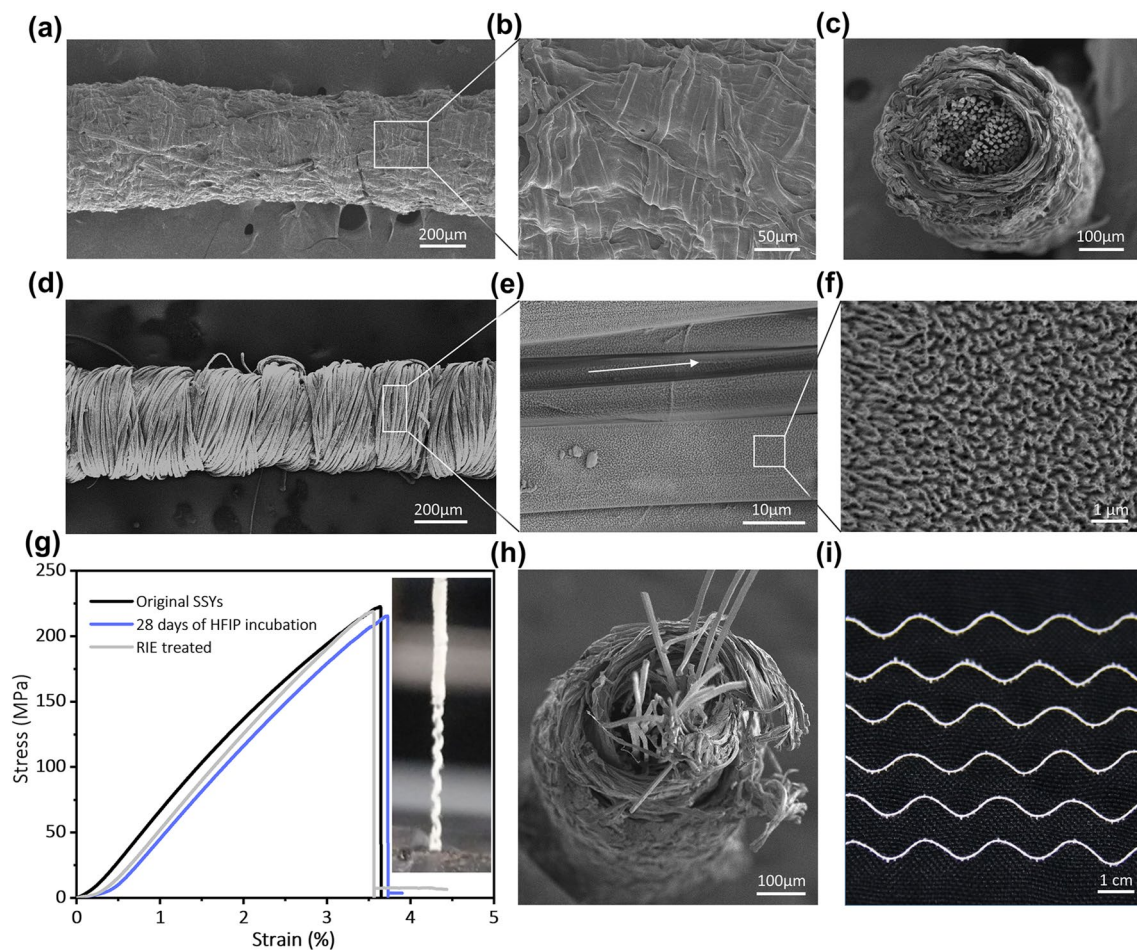


**Fig. 2** Morphology and mechanical property of modified SSYs. **a** SEM image of surface morphology of SSY after incubated in HFIP for 14 days. **b** Higher magnification image of (a). **c** SEM image of cross-section of (a), by knife cutting. **d** SEM image of surface morphology of SSY after 10 min ion etching. **e** Higher magnification SEM image of (d). **f** Higher magnification SEM image of (e). **g** Typi-

cal stress-strain curves of SSYs, HFIP incubated SSYs (28 days) and ion etched SSYs (10 min), respectively. Insert: image of an SSY after mechanical failure, showing the outer layer is remained. **h** Cross-section SEM image of an HFIP incubated SSYs (28 days) after mechanical failure, while the attached outer layer has been cut. **i** A wavy pattern of SSYs weaved on a fabric by an automatic embroidery machine

surface gradually faded. The adjacent silk fibers interfaces are first disappeared, and at last, the helical morphology will become a smooth and isotropic surface morphology (60 °C for 28 days, Fig. S2c). Besides, the effect of HFIP takes place from the surface of silk layer due to the compact wrapping: the silk fibers inside the wrapping layer can still be observed while the fiber/fiber interface has become indistinct (60 °C for 14 days, Fig. 2c). Therefore, the diameter of SSY shows no significant change even most silk fibers at the surface have been dissolved (Fig. S2).

While partial dissolution process increases the inter connections in the silk fiber layer, the surface roughness of SSYs is reduced. However, the surface roughness is usually preferred during applications, especially in TENG systems. Nanostructures were introduced into the SSY surface through RIE treatment to enhance surface roughness. A uniform lawn-like surface composed by the nanofibrillar structures were created on surface silk fibers by RIE as described in the experimental section (Fig. 2d–f). The etched thickness and the morphologies of the nanofibrils were tuned through controlling the processing conditions (Fig. S3). Nanostructures can be created even at a rapid etching time of 5 minutes. Moreover, the length of the nanowire increases with the increasing of processing time. The reactive ion etching is a nano-fabrication method, therefore, the overall macro morphology of SSYs is not influenced (Fig. 2d).

Both partial dissolution and reactive ion etching process will not impact the inner stainless-steel core fiber. In fact, as shown in Fig. S4, the stainless-steel core fiber demonstrates a much stronger strength than the silk fibers (tensile force at fracture  $26.3 \pm 3.1$  N for stainless-steel fiber and  $2.2 \pm 0.3$  N for silk fibers, respectively). So, the mechanical property of SSYs is mainly determined by the stainless-steel core. SSYs shows a tensile strength of  $223 \pm 16$  MPa and toughness of  $3.9 \pm 0.5$  MJ m<sup>-3</sup>, while the modified SSYs, both partial dissolved and reactive ion etched, show no significant difference in this respect (Fig. 2g), which are comparable to other high-performance functional fibers [23, 24]. Although the wrapped silk fiber layer does enhance the mechanical strength of SSYs, the helical arranged outer layer provides a structure maintain function when the inner core fractures or even breaks completely (insert picture in Fig. 2g). The cross-sectional SEM image further indicates that the stainless-steel fiber core remains compacted after mechanical tensile failure, due to the high lateral force provided by the wrapped silk fibers (Fig. 2h). As a result, the produced SSYs show excellent processability. They can be directly weaved by an automatic embroidery machine (Fig. 2i).

### Preparation a Stretchable TENG Cable

Stretchable TENG cables were fabricated by using the prepared SSYs as one electrode, and a silicone rubber tube

winding with copper wire as the other electrode (Fig. 3a). For TENGs, the contact-and-separate of electrically positive and negative materials trigger the current in the external circuit. For the SSYs, the sheath silk fibers have been proven a promising triboelectric positive material, while the stainless-steel core provides a good conductivity for charge transfer. Almost all materials have a triboelectrification effect, but their ability to gain and lose electron is different, which depends on their polarity. Silks have a strong trend to lose electrons and become positively charged when rub with other materials. By checking “triboelectric series” [25–27] which is an ordering of materials according to their tendency to develop a positive or negative charge, silicone rubber tube was selected. Firstly, silicone rubber tube can ensure an adequate charge transfer when contact-and-separate with silks. Secondly, silicone rubber tubes show an excellent stretchability with good tensile recoverability (can be stretched to 100% with no obvious tensile fatigue) (Fig. S5). The latter of which is particularly significant for long-time use of the TENG cables.

By using the core-sheath spring structure, contact-and-separate of the SSYs and silicone rubber tube can be achieved by release-and-stretch of the TENG cable. For an as prepared TENG cable, the SSYs is settled inside the silicone rubber tube, with a spiral structure and attaching to the inner wall of the silicone rubber tube (Fig. 3b). When stretch the cable, the spiral SSY will be straightened. Since the diameter of SSYs is much smaller than the silicone rubber tube, the straightened SSY will be de-attached from the silicone rubber tube wall (Fig. 3c). Besides, copper wire is also in a spiral shape and attached on the outside of silicone rubber tube for charge transfer in the negative electrode, which will always attach on the outer wall of the silicone rubber tube even being stretched to 100% (Fig. S6).

Working principle of the TENG cable under stretch-and-release is demonstrated in Fig. 4a. Basically, the positive material, silks on the SSY, tend to loss electrons during contact with the negative material, silicone rubber tube, which tend to obtain electrons. The charge separation happens during the fabrication process of a TENG cable (Fig. 4a). By pre-stretching the silicone rubber tube and releasing together with the inner SSY, a spiral structure is formed. When the two materials with different electron-attracting abilities get contact at the first time, an electric potential will be formed between the two interfaces [28]. Once they are separated, the alternative potential will drive electrons in the outer circuit to flow back and forth to balance the potential. From another point of view, in an as fabricated TENG cable, the SSY is in the spiral state and is contacted with the silicone rubber inner wall. When stretched the device, SSY is strengthened and separated with the silicone rubber inner wall. Therefore, during one stretch-and-release process, current will be generated in the external circuit twice in opposite directions.

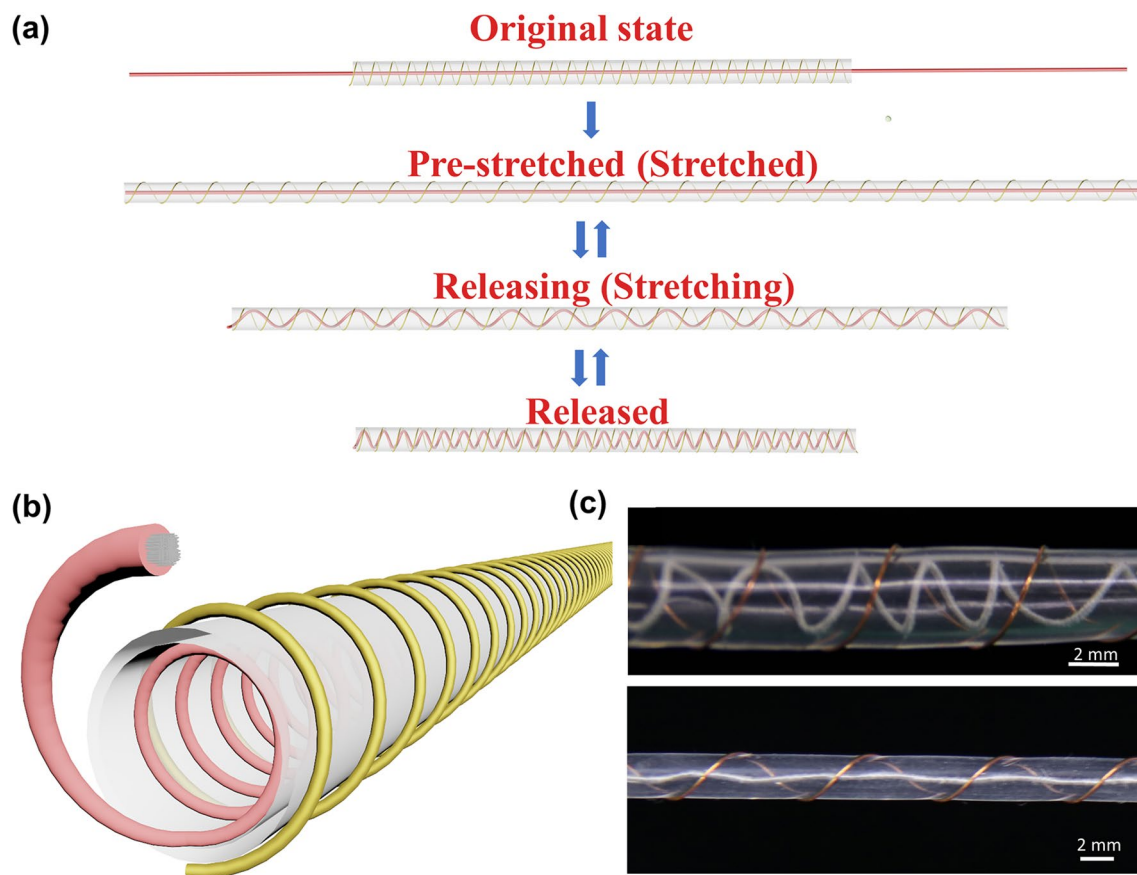


**Fig. 3** Preparation and structures of a stretchable TENG cable. **a** Schematic diagram of the fabrication of TENG cables. **b** 3D sketch of the assembled TENG cable. **c** Photograph of the assembled TENG cable at released (top) and 100% stretched (below) state

Electrical output performance of the TENG cables was further evaluated (Fig. 4b–d). The output voltage peak of a 15 cm TENG cable on 500 M $\Omega$  loading resistance reached up to  $\sim 2.8$  V when being stretched to 50% (Fig. 4b). The output voltage peak was reduced with the decreased stretching ratio. However,  $\sim 0.2$  V was maintained even at a low stretch of 13%. On the other hand, the output voltage peak was increased by the working frequency (Fig. 4c), which increases from  $\sim 0.7$  to  $\sim 1.6$  V while the work frequency increases from 0.5 to 1.85 Hz on an external loading of 500 M $\Omega$  and tensile strain of 25%. The relation between the voltage and the transfer time (or frequency) on this condition can be estimated through the equation of  $V = QR/t$ . Here, the transfer charge ( $Q$ ) generated by each contact at different frequency can be regarded as a constant at the stable contact-separation mode. Accordingly, this equation reveals that the higher working frequency [namely less charge transfer time ( $t$ )] can result in faster charge transfer between two electrodes of the TENG cable and thereby lead to the increase of the output voltage on a certain external load.

Energy output stability of the TENG cables was evaluated by 20,000 cycle repeated stretch-and-release tests of

a 15 cm TENG cable. As shown in Fig. 4d, short-circuit current of the TENG cable during 20,000 cyclic test shows no decrease as test time goes on, indicating good stability of TENG cables. In regular TENG systems, the charge density on the two electrode surfaces will be saturated within several contacts [29]. However, for TENG cables, the contact region between core SSY and sheath silicone rubber tube is not exactly constant, and the contact force is small. As a result, the charge density on the two surfaces needs sufficient contacts to reach the saturated state. Therefore, short-circuit current of the TENG cable shows an increasing trend during cyclic test. Electrical output performance of TENG cables based on modified SSYs were also tested. All of the TENG cables based on different modified SSYs were fixed at 10 cm in length and tested with 100% tensile strain at a working frequency of 0.6 Hz. As expected, SSYs with a smoother surface morphology showed a decreased output voltage peak from  $\sim 2.5$  to  $\sim 1.7$  V after 28 days HPIF incubation, while the 10 min ion etched SSYs showed an increased output voltage peak up to above 3.0 V (Fig. 4e, f). These results correspond to the widely accepted principle that nanostructures on the electrode surface is beneficial for increasing

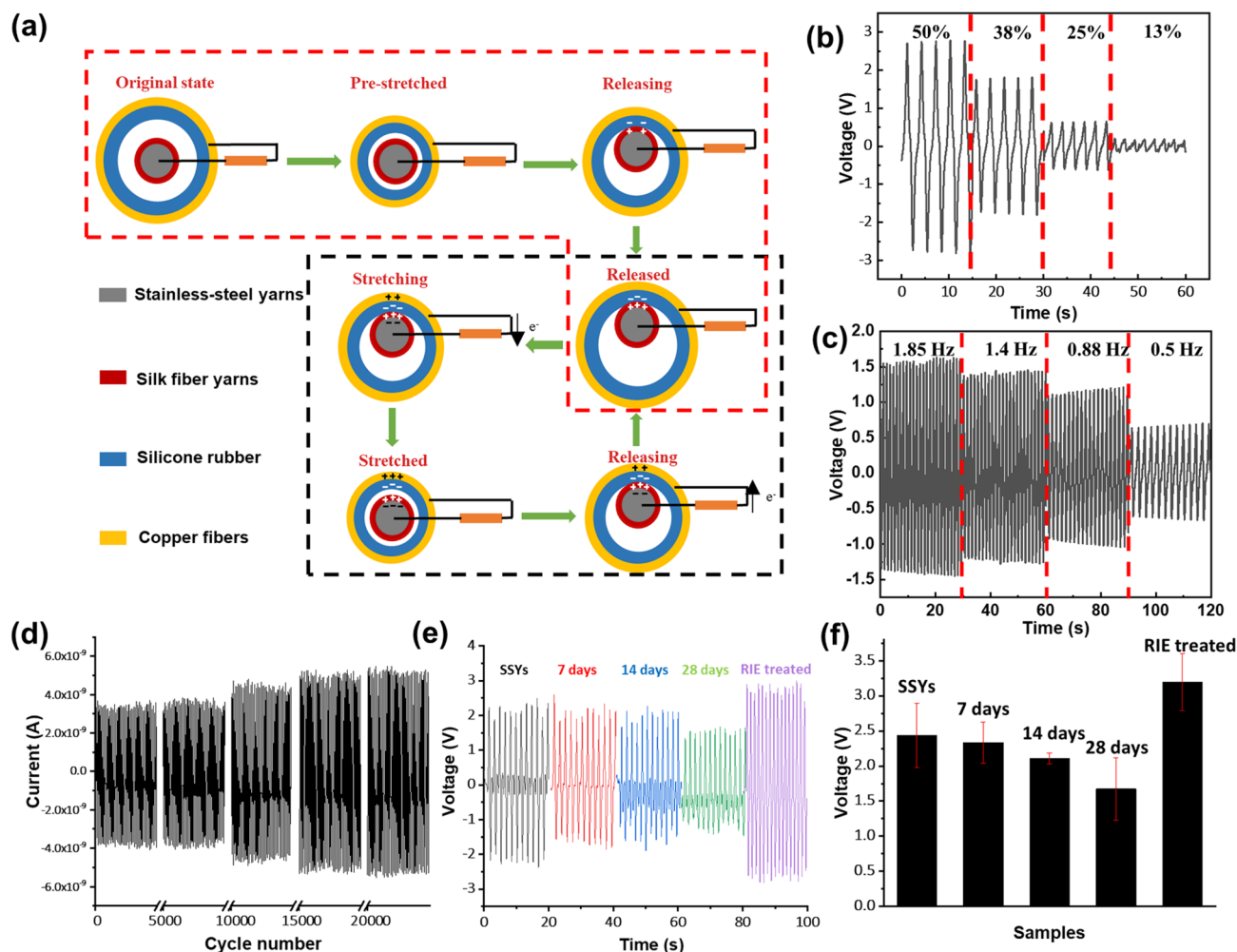


**Fig. 4** Electrical output performance of TENG cables. **a** Schematic illustration of working principle of the TENG cable, red dotted box indicates the fabrication process of the TENG cable, black dotted box indicates the cyclic working process of the TENG cable. **b** Measured output voltage of the TENG cable on the external loading of 500 M $\Omega$  under different stretch ratio (cable length: 15 cm). **c** Measured output voltage of the TENG cable on the external loading of 500 M $\Omega$  at dif-

ferent work frequencies (cable length: 15 cm). **d** short-circuit current of the TENG cable during 20,000 cyclic tests on working frequency of 2.5 Hz (cable length: 10 cm). **e** Measured output voltage of TENG cables based on different SSYs (SSYs, HFIP incubated SSYs with different days and RIE treated SSYs) with the external loading of 500 M $\Omega$  (cable length: 10 cm). **f** Quantitative comparison of (e)

the contact area and will further improve the output voltage value. Further, the durability of the output performance of TENG cables based on RIE-treated SSYs was evaluated by a long-term cyclic test. As shown in Fig. S7, their short-circuit current showed no obvious reduction during 6000 cycles and maintained ~80% after 10,000 cycles.

### Applications of SSYs and TENG Cables for Wearable Electronics

SSYs are designed especially for wearable applications, such as conducting wires for electronic devices integrated cloth, real-time energy harvesting and self-powered sensors (Fig. 5a). Herein, several examples are presented. Due to

the excellent weave-ability, SSYs can perfectly integrated with cloth without affecting the comfort of wearing. The stainless-steel core provides excellent conductivity while the wrapped silk layer provides a good protection, enable the resulted SSYs with an outstanding stability which can easily tolerate washing machine cleaning and drying process (Fig. 5b). Further, the TENG cables can be integrated in series or parallel and woven into a power textile (Fig. 5c). Since the TENG cables also provide a rapid responsive ability to stretching with different frequency and extent, they can be used for real-time movement monitoring (Fig. 5d).

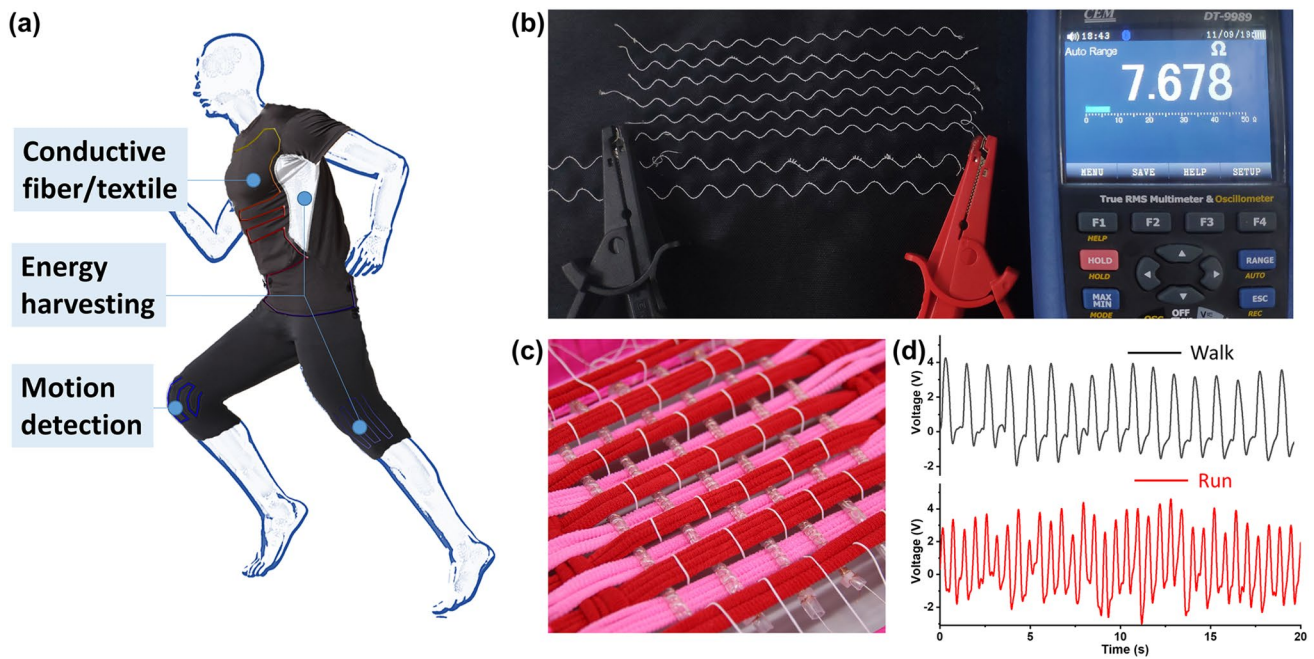


**Fig. 5** Application of SSYs and TENG cables. **a** Schematic illustration of application of TENG cables. **b** Resistance test of the cloth integrated with SSYs after washing machine cleaning and drying pro-

cess. **c** Photograph of the TENG cables woven into a power textile. **d** Output signals of the TENG cables integrated in a kneecap when monitoring movement.

## Discussion

The SSYs produced in this work show preferred mechanical property for modern textile technology, and good structural stability in practical long-term use. Compared with circuit printed on a cloth and conventional conductive metal wires protected by polymer insulation layer [30], SSYs shows superiorities: wrapped silk sheath layer is more reliable, which can tolerate machine operations and washing process, especially for the HFIP treated SSYs. The introduced interfacial connections between silk bundles enhance the stabilities without affecting the overall flexibility of SSYs. As the surface layer which might be directly in touch with human skin, silks reveal excellent wearing comfort because they have been a popular clothing material for thousands of years [31–33]. However, compared with synthetic polymer sourced TENGs, the good hydrophilicity of silk might lead to a reduced charge generation in a humid environment for silk sourced TENGs, which causes reduced output performance. Surface hydrophobic modification of silk can be used to optimize silk sourced TENGs. RIE treatment has been proved to be able to create micro-nano structures on the surface of silk, which could improve hydrophobic of silk due to lotus effect. Further, surface grafting treatment can also be used to improve hydrophobic of silk by introducing hydrophobic group. The environmentally friendly co-wrapping spinning to produce SSYs also provide a universal

technique to produce conductive wires for e-textiles with low cost and high efficiency. Different conductive wires can be wrapped with different type of traditional textile fiber. But the mechanical properties of core and sheath fibers have to be matched. For example, if the core fiber is very soft while the sheath fiber is relatively tough, more technical problems will need to be solved.

TENG cables fabricated in this work showed energy harvesting ability and stretch responsiveness. In terms of the device fabrication, although the surface modification processes of SSYs have been proven effective for regulating the device performance, the spiral structure also plays a crucial role [18, 34]. The SSY core develops into spiral structure in the sheath tube during the recovery of 100% pre-stretching in this work. The number of spiral circles of SSY core can be further increased by larger pre-stretching, which can create a larger contact area between core yarn and sheath tube, and finally result in an improved electrical output performance of TENG cables. However, if a TENG cable contained too much SSY spiral in the tube, its responsiveness to small extent of stretch would decrease. Therefore, the specific amount of core fiber in the TENG cable is depend on the application requirement, whether they are used as power source or used as motion detector.

SSYs can also be directly woven into fabrics to build fabric type generators. The overall surface area can be increased by ion etching. However, in practical applications,



nanostructures are easy to be worn. Proper solvent treatment can improve the stability of the structure and maintain the original micro-scale rough structure introduced by helical wrapping process. The latter is considered to be a more favorable choice for industrial application.

## Conclusions

In summary, stretchable TENG cables were fabricated based on SSYs, which provide not only energy harvesting function but also self-powered tension sensor function. This type of core-sheath conductive yarns can be produced by simple co-wrapping spinning technique. The continuously lab produced SSYs show good mechanical properties and weavability and can be further modified to control their surface structure from nanoscale to macroscale. Both SSYs and they based TENG cables are suggested to have promising application potentials in multifunctional devices integrated smart cloth.

**Acknowledgements** The authors thank Xue Chen and Zhen Wang for drawing the wonderful violin image and TENG cable image. SEM characterization was performed at the Center for High-resolution Electron Microscopy (ChEM) at the School of Physical Science and Technology (SPST), ShanghaiTech University. This work was supported by the National Natural Science Foundation of China (No. U1832109, 21808220, 81700227), Shanghai Pujiang Program (18PJ1408600), the starting grant of ShanghaiTech University, Shanghai Sailing Program (17YF1411500) and Shanghai Rising-Star Program (18QA1403000).

## Compliance with Ethical Standards

**Conflict of interest** The authors declare no competing interests.

## References

- Ye C, Ren J, Wang Y, Zhang W, Qian C, Han J, et al. Design and fabrication of silk templated electronic yarns and applications in multifunctional textiles. *Mater*. **2019**;1(5):1411–25.
- Shi Q, Sun J, Hou C, Li Y, Zhang Q, Wang H. Advanced functional fiber and smart textile. *Adv Fiber Mater*. **2019**;1(1):3–31.
- Cao R, Pu X, Du X, Yang W, Wang J, Guo H, et al. Screen-printed washable electronic textiles as self-powered touch/gesture tribo-sensors for intelligent human-machine interaction. *ACS Nano*. **2018**;12(6):5190–6.
- Hota MK, Jiang Q, Wang Z, Wang ZL, Salama KN, Alshareef HN. Integration of electrochemical microsupercapacitors with thin film electronics for on-chip energy storage. *Adv Mater*. **2019**;31(25):1807450.
- Zhang Z, Wang L, Li Y, Wang Y, Zhang J, Guan G, et al. Nitrogen-doped core-sheath carbon nanotube array for highly stretchable supercapacitor. *Adv Energy Mater*. **2017**;7(5):1601814.
- Ren J, Bai W, Guan G, Zhang Y, Peng H. Flexible and weavable capacitor wire based on a carbon nanocomposite fiber. *Adv Mater*. **2013**;25(41):5965–70.
- Ren J, Zhang Y, Bai W, Chen X, Zhang Z, Fang X, et al. Elastic and wearable wire-shaped lithium-ion battery with high electrochemical performance. *Angew Chem*. **2014**;126(30):7998–8003.
- Dong K, Wang Y, Deng J, Dai Y, Zhang S, Zou H, et al. A highly stretchable and washable all-yarn-based self-charging knitting power textile composed of fiber triboelectric nanogenerators and supercapacitors. *ACS Nano*. **2017**;11(9):9490–9.
- Balilonda A, Li Q, Tebyetekerwa M, Tusiime R, Zhang H, Jose R, et al. Perovskite solar fibers: current status, issues and challenges. *Adv Fiber Mater*. **2019**;1(2):101–25.
- Zhu L, Wang ZL. Recent progress in piezo-phototronic effect enhanced solar cells. *Adv Funct Mater*. **2019**;29(41):1808214.
- Wang J, Li X, Zi Y, Wang S, Li Z, Zheng L, et al. A flexible fiber-based supercapacitor-triboelectric-nanogenerator power system for wearable electronics. *Adv Mater*. **2015**;27(33):4830–6.
- Ye C, Dong S, Ren J, Ling S. Ultrastable and high-performance silk energy harvesting textiles. *Nano-Micro Lett*. **2019**. <https://doi.org/10.1007/s40820-019-0348-z>.
- Wang ZL. Entropy theory of distributed energy for internet of things. *Nano Energy*. **2019**;58:669–72.
- Cao X, Jie Y, Wang N, Wang ZL. Triboelectric nanogenerators driven self-powered electrochemical processes for energy and environmental science. *Adv Energy Mater*. **2016**;6(23):1600665.
- Zhou T, Zhang C, Han C, Fan F, Tang W, Wang ZL. Woven structured triboelectric nanogenerator for wearable devices. *ACS Appl Mater Interfaces*. **2014**;6(16):14695–701.
- Zhong J, Zhang Y, Zhong Q, Hu Q, Hu B, Wang Z, et al. Fiber-based generator for wearable electronics and mobile medication. *ACS Nano*. **2014**;8(6):6273–80.
- Dong K, Peng X, Wang ZL. Fiber/fabric-based piezoelectric and triboelectric nanogenerators for flexible/stretchable and wearable electronics and artificial intelligence. *Adv Mater*. **2019**;31:1902549.
- Gong W, Hou C, Guo Y, Zhou J, Mu J, Li Y, et al. A wearable, fibroid, self-powered active kinematic sensor based on stretchable sheath-core structural triboelectric fibers. *Nano Energy*. **2017**;39:673–83.
- Haas R, Degischer HP, Pongratz P, Pyzalla AR. Microstructure and properties of violin strings made of metastable austenitic steel. *Int J Mater Res*. **2009**;100(11):1557–1565.
- Ling S, Qin Z, Li C, Huang W, Kaplan DL, Buehler M J Polymorphic regenerated silk fibers assembled through bioinspired spinning. *Nat Commun*. **2017**;8:12.
- Ling S, Li C, Jin K, Kaplan DL, Buehler MJ. Liquid exfoliated natural silk nanofibrils: applications in optical and electrical devices. *Adv Mater*. **2016**;28:7783–90.
- Ling S, Jin K, Kaplan DL, Buehler MJ. Ultrathin free-standing bomyx mori silk nanofibril membranes. *Nano Lett*. **2016**;16(6):3795–800.
- Zhang J, Liu JW, Zhuang RC, Mader E, Heinrich G, Gao S. Single MWNT-glass fiber as strain sensor and switch. *Adv Mater*. **2011**;23(30):3392.
- Hu Y, Cheng H, Zhao F, Chen N, Jiang L, Feng Z, et al. All-in-one graphene fiber supercapacitor. *Nanoscale*. **2014**;6(12):6448–51.
- Henniker J. Triboelectricity in polymers. *Nature*. **1962**;196(4853):474–4.
- Wang ZL. Triboelectric nanogenerators as new energy technology for self-powered systems and as active mechanical and chemical sensors. *ACS Nano*. **2013**;7(11):9533–57.
- Zou H, Zhang Y, Guo L, Wang P, He X, Dai G, et al. Quantifying the triboelectric series. *Nat Commun*. **2019**;10(1):1427.
- Wang ZL, Wang AC. On the origin of contact-electrification. *Mater Today*. **2019**;30:34–51.

29. Wang ZL. On Maxwell's displacement current for energy and sensors: the origin of nanogenerators. *Mater Today*. **2019**;20(2):74–82.
30. Zhang M, Zhao M, Jian M, Wang C, Yu A, Yin Z, et al. Printable smart pattern for multifunctional energy-management e-textile. *Matter*. **2019**;1(1):168–79.
31. Vepari C, Kaplan DL. Silk as a biomaterial. *Prog Polym Sci*. **2007**;32(8–9):991–1007.
32. Zhang W, Ye C, Zheng K, Zhong J, Tang Y, Fan Y, et al. Tensan silk-inspired hierarchical fibers for smart textile applications. *ACS Nano*. **2018**;12(7):6968–77.
33. Hu T, Kaplan DL, Omenetto FG. Silk materials—a road to sustainable high technology. *Adv Mater*. **2012**;24(21):2824–37
34. Dong K, Deng J, Ding W, Wang AC, Wang P, Cheng C, et al. Versatile core–sheath yarn for sustainable biomechanical energy harvesting and real-time human-interactive sensing. *Adv Energy Mater*. **2018**;8(23):1801114.



**Chao Ye** received his B.S. degree in Nonwoven Materials and Engineering from Soochow university in 2017 and he is currently perusing a Ph.D. from ShanghaiTech University. His researches focus on fiber sensors and smart textiles.



**Quanfu Xu** is currently an attending doctor in Xinhua hospital affiliated to School of medicine, Shanghai Jiao Tong university. His research focuses on the applications of advanced materials in cardiovascular disease and health monitoring. He obtained his M.D. degree from the First Military Medical University (2006) and Ph.D. from Shanghai Jiao Tong University School of Medicine (2012). During 2010–2012, He awarded the State Scholarship Fund of China to pursue his study at Goethe University, Frankfurt am Main, Germany, as a joint Ph.D. student.



materials for wearable applications.

**Jing Ren** is currently a Research Assistant Professor in the School of Physical Science and Technology at ShanghaiTech University. She received her B.S. in Chemistry at Lanzhou University in China in 2007, Ph.D. in Macromolecular Chemistry and Physics at Fudan University in China in 2016. She then worked at Xinhua Hospital Affiliated to Shanghai Jiaotong University School of Medicine before joining ShanghaiTech University in 2018. She focuses on the development of functional natural



**Shengjie Ling** is an assistant professor in the School of Physical Science and Technology at ShanghaiTech University. His research focuses on developing biopolymer functional materials through the integration of synchrotron-based characterization, computational modeling and bioinspired & biomimetic fabrication. He obtained his B.S. degree from the Zhejiang University of Technology (2009) and Ph.D. from Fudan University (2014). During 2012–2013, He awarded the State Scholarship Fund of China to pursue his study at ETH Zurich, Switzerland, as a joint Ph.D. student. Prior to joining ShanghaiTech University, he worked as a postdoctoral associate at MIT and Tufts University (2014–2017).